

Orbital Architectures of Planet-Hosting Binaries: I. Forming Five Small Planets in the Truncated Disk of Kepler-444A*

Trent J. Dupuy,¹ Kaitlin M. Kratter,² Adam L. Kraus,¹ Howard Isaacson,³ Andrew W. Mann,¹
Michael J. Ireland,⁴ Andrew W. Howard,⁵ and Daniel Huber⁶

ABSTRACT

We present the first results from our Keck program investigating the orbital architectures of planet-hosting multiple star systems. Kepler-444 is a metal-poor triple star system that hosts five sub-Earth-sized planets orbiting the primary star (Kepler-444A), as well as a spatially unresolved pair of M dwarfs (Kepler-444BC) at a projected distance of $1''.8$ (66 AU). We combine our Keck/NIRC2 adaptive optics astrometry with multi-epoch Keck/HIRES RVs of all three stars to determine a precise orbit for the BC pair around A, given their empirically constrained masses. We measure minimal astrometric motion (1.0 ± 0.6 mas yr⁻¹, or 0.17 ± 0.10 km s⁻¹), but our RVs reveal significant orbital velocity (1.7 ± 0.2 km s⁻¹) and acceleration (7.8 ± 0.5 m s⁻¹ yr⁻¹). We determine a highly eccentric stellar orbit ($e = 0.864 \pm 0.023$) that brings the tight M dwarf pair within $5.0_{-1.0}^{+0.9}$ AU of the planetary system. We validate that the system is dynamically stable in its present configuration via n-body simulations. We find that the A-BC orbit and planetary orbits are likely aligned (98%) given that they both have edge-on orbits and misalignment induces precession of the planets out of transit. We conclude that the stars were likely on their current orbits during the epoch of planet formation, truncating the protoplanetary disk at ≈ 2 AU. This truncated disk would have been severely depleted of solid material from which to form the total $\approx 1.5 M_{\oplus}$ of planets. We thereby strongly constrain the efficiency of the conversion of dust into planets and suggest that the Kepler-444 system is consistent with models that explain the formation of more typical close-in *Kepler* planets in normal, not truncated, disks.

*Data presented herein were obtained at the W.M. Keck Observatory, which is operated as a scientific partnership among the California Institute of Technology, the University of California, and the National Aeronautics and Space Administration. The Observatory was made possible by the generous financial support of the W.M. Keck Foundation.

¹The University of Texas at Austin, Department of Astronomy, 2515 Speedway C1400, Austin, TX 78712, USA

²Department of Astronomy, University of Arizona, 933 N Cherry Ave, Tucson, AZ, 85721

³Astronomy Department, University of California, Berkeley, CA 94720, USA

⁴Research School of Astronomy & Astrophysics, Australian National University, Canberra ACT 2611, Australia

⁵Institute for Astronomy, University of Hawaii, 2680 Woodlawn Drive, Honolulu HI 96822

⁶Sydney Institute for Astronomy, School of Physics, University of Sydney, NSW 2006, Australia

Subject headings: astrometry — binaries: close — planetary systems — stars: individual (Kepler-444)

1. Introduction

The demographics of planets around single stars have been studied extensively for two decades, but statistical studies of planets in binary systems have been hampered by observational selection effects. The *Kepler* prime mission (Borucki et al. 2010) has produced the first large sample of planet detections that are minimally biased with respect to the multiplicity of the stellar hosts. While *Kepler* data has been used to identify a number of circumbinary planets (e.g., Doyle et al. 2011; Welsh et al. 2012), high-angular resolution surveys of *Kepler* planet candidate hosts have been needed to discover so called “s-type” planets that orbit only one star in a multiple star system. Such work has aided in planet validation (e.g., Adams et al. 2012, 2013; Lillo-Box et al. 2014; Everett et al. 2015), and studies of the binary frequency in the *Kepler* planet sample have also provided the first constraints on how planet occurrence is affected by the presence of stellar companions (Wang et al. 2014, 2015; Kraus et al., submitted to AJ). However, the impact of stellar multiplicity on planet formation and system architecture depends not simply on the presence of a companion but on orbital parameters such as eccentricity and mutual inclination.

Theoretical work on the formation of planets in binaries preceded their discovery by many decades (e.g., Heppenheimer 1974). Companion stars are expected to both excite the random velocities of planetesimals, inhibiting their growth to large sizes, and truncate protoplanetary disks due to tidal effects (Artymowicz & Lubow 1994). These effects were long thought to inhibit planet formation in binary systems where the semimajor axis is comparable to the disk radius. Indeed, observations of the occurrence of protoplanetary disks among single stars versus binaries has shown that disks exist but are much less common among <40 AU binaries (e.g., Ghez et al. 1997; White & Ghez 2001; Cieza et al. 2009; Kraus et al. 2011, 2012). In addition, Harris et al. (2012) showed that when the individual components of binaries host protoplanetary disks, their masses are depleted by a factor of ~ 5 for 30–300 AU binaries and ~ 25 for <30 AU binaries. Despite such hostile factors, some planet hosting binary systems exist, e.g., γ Cep that has a 20 AU binary semimajor axis and a $2 M_{\text{Jup}}$ planet at 2 AU (Hatzes et al. 2003). Theoretical studies of the γ Cep system have shown that even the truncated disk mass was plausibly large enough to accommodate giant planet formation (Jang-Condell et al. 2008). More general theoretical work (Rafikov 2015; Silsbee & Rafikov 2015) demonstrates that planet formation may occur in binaries if planetesimals are either large, as expected from streaming instabilities (Youdin & Goodman 2005), or if the birth disk is massive enough to damp random planetesimal velocities. However, these successful theories do not anticipate the extreme dynamical environment we describe here.

We present the first results of our campaign to observationally determine the orbital architec-

tures of the stellar multiples that host *Kepler* planets by measuring their orbital motion. Kepler-444 (a.k.a. BD+41 3306, HIP 94931, KOI-3158) was discovered by Lillo-Box et al. (2014) to have a $1''.8$ companion, corresponding to a projected separation of 66 AU given the *Hipparcos* parallactic distance of $35.7_{-1.1}^{+1.0}$ pc (van Leeuwen 2007). Campante et al. (2015) validated that the five *Kepler* candidates are sub-Earth radius planets ($0.40\text{--}0.74 R_{\oplus}$) orbiting the primary star Kepler-444A and reported that the companion is in fact a double-lined spectroscopic binary itself, which we denote Kepler-444BC. Campante et al. (2015) also used asteroseismology of Kepler-444A to derive stellar parameters including system an age of 11.2 ± 1.0 Gyr, which they note is consistent with kinematic and compositional evidence for the star being a member of the thick disk. While three other hierarchical triple systems are known to host planets, the stellar companions have much larger projected separations from the host stars (240–330 AU; Bechter et al. 2014; Eastman et al. 2015) and no others are known to host multi-planet systems.

In this paper we combine astrometric and radial velocity (RV) observations to show that the orbit of the M dwarf pair Kepler-444BC’s center of mass around the planet hosting star Kepler-444A (hereinafter called the “A–BC orbit”) is highly eccentric with a closest approach of 5 AU. We discuss why this orbital configuration is likely primordial and how it is expected to have strongly impacted the protoplanetary disk that formed the planetary system around Kepler-444A. We review plausible formation scenarios for this peculiar system.

2. Observations

2.1. Keck/NIRC2 AO Imaging

We monitored the Kepler-444 system with the natural guide star (NGS) adaptive optics (AO) system at Keck II (Wizinowich et al. 2000) from 2013 Aug 7 UT to 2015 Apr 11 UT. We obtained data with the facility imager NIRC2 in both the standard Mauna Kea Observatories K' band and the narrow-band filter K_{cont} ($\lambda_{\text{cent}} = 2.2705 \mu\text{m}$, $\Delta\lambda = 0.0296 \mu\text{m}$). Our images were reduced in a standard fashion, performing linearity correction, bias subtraction, flat fielding, and correction of bad pixels and cosmic rays as described in Kraus et al. (submitted to AJ). We used StarFinder PSF-fitting (Diolaiti et al. 2000) to measure the precise positions of the two components, as in our previous work on Keck AO imaging of binaries (e.g., Dupuy et al. 2009, 2010, 2014). Examining the residuals of our fits we found no evidence for any other resolved components in the system (Figure 1). Thus we place a limit of ≈ 10 mas on the separation of the Kepler-444BC pair at all three epochs, implying a semimajor axis of $\lesssim 0.3$ AU.

To convert (x, y) measurements in individual exposures to positions on the sky we first corrected for the optical distortion of NIRC2 using the Yelda et al. (2010) calibration, applying their pixel scale of $9.952 \text{ mas pixel}^{-1}$ and $+0.252$ correction for the orientation given in the NIRC2 image headers. Our NIRC2 data from 2013 and 2014 were obtained in vertical angle mode, where the sky rotation of the images is constantly changing, so we corrected the rotator angles reported in those headers

to correspond to the midpoint instead of the start of the exposure. We then applied corrections for differential aberration and atmospheric refraction. The refraction correction requires knowledge of the air temperature, pressure, and humidity on Mauna Kea during our observations, for which we used the weather data archived by the Canada-France-Hawaii Telescope.¹ In K' band, this refraction correction varies slightly between Kepler-444A and Kepler-444B because their K -band spectra result in a small difference in the effective wavelength (λ_{eff}) of our observations. To compute these wavelengths we convolved the NIRC2 K' -band filter curve² with spectra representative of the two components. We used the IRTF Spectral Library³ spectrum of HD 145675 (K0V) as a template for Kepler-444A and the actual observed spectrum of Kepler-444B from IRTF/Spex (A. Mann private communication, 2015) and found flux-weighted average wavelengths of $\lambda_{\text{eff}} = 2.1089 \mu\text{m}$ and $2.1184 \mu\text{m}$, respectively.

Table 1 gives our final separation and position angle (PA) measurements from NIRC2. The errors quoted in Table 1 are simply the rms of measurements obtained from multiple individual exposures, but there are other potential sources of systematic error in this astrometry. The pixel scale and orientation have been shown at times to vary between epochs at the $0.002 \text{ mas pixel}^{-1}$ and $0^\circ 009$ level.⁴ The scale uncertainty would correspond to a systematic error of 0.37 mas in separation here. In addition, it is possible that photocenter shifts due to the orbital motion of the components of Kepler-444BC about their center of mass could affect our (unresolved) NIRC2 astrometry of this source, although as we derive in Section 2.2 this is expected to be a relatively small ($<0.3 \text{ mas}$) effect.

Our relative astrometry for Kepler-444AB shows only marginal evidence for orbital motion. Thus, to assess our total astrometric uncertainties, we fit linear relations to both separation and position angle (PA) as a function of time and adopted the standard deviation (rms) of the residuals as our final errors. We find an rms about of the fit of 0.44 mas in separation and $0^\circ 023$ in PA, consistent with known sources of systematic error discussed above. We find a slight trend of decreasing separation ($-1.0 \pm 0.3 \text{ mas yr}^{-1}$) and no evidence for change in PA ($-0.002 \pm 0.017 \text{ deg yr}^{-1}$), as shown in Figure 2. Combining these two linear trends and their uncertainties, the total astrometric motion is $1.0 \pm 0.6 \text{ mas yr}^{-1}$. At a distance of 35.7 pc , these marginal astrometric motion detections correspond to $0.17 \pm 0.05 \text{ km s}^{-1}$ in separation and $0.01 \pm 0.09 \text{ km s}^{-1}$ in PA (total motion of $0.17 \pm 0.10 \text{ km s}^{-1}$). This is much smaller than, for example, the 4.2 km s^{-1} relative velocity of a circular 66 AU binary with $M_{\text{tot}} = 1.3 M_{\odot}$. We also note that this almost negligible change in

¹<http://mkwc.ifa.hawaii.edu/archive/wx/cfht/>

²<http://www2.keck.hawaii.edu/inst/nirc2/filters.html>

³http://irtfweb.ifa.hawaii.edu/~spex/IRTF_Spectral_Library/

⁴Examining Table 4 in Yelda et al. (2010) shows that given their measurement uncertainties epoch-to-epoch variations in scale and orientation are indeed significant in a χ^2 sense, where $p(\chi^2) = 2.8 \times 10^{-3}$ for the pixel scale and $p(\chi^2) = 1.0 \times 10^{-6}$ for the orientation. In contrast, Yelda et al. (2010) performed tests to show that there is no evidence of time variations in their distortion solution.

the relative astrometry between Kepler-444A and Kepler-444BC confirms that this is a physically bound system, since the primary star’s proper motion is 640 mas yr^{-1} .

2.2. Keck/HIRES RVs

We obtained spectra of Kepler-444A with the HIRES spectrometer on the Keck I Telescope from 2012 July to 2015 July. The standard setup of the California Planet Search (Howard et al. 2010) was used in order to maintain high precision of the radial velocities. During our first observation of Kepler-444A, we identified the unresolved M dwarf companion Kepler-444BC $\approx 2''$ away from the primary. At all epochs we positioned the decker such that light from the companion did not contaminate the spectra of the primary. If the seeing conditions deteriorated to greater than $1''0$ and the two stars could not be isolated from each other, then the star was not observed. Each observation was taken through the gas cell of molecular iodine (I_2) with typical exposure times of 300s. An iodine free exposure was also obtained in order to compute radial velocities with the forward modeling technique as described in Butler et al. (2006). We report our relative RVs for Kepler-444A in Table 2, and we found an absolute RV of $-121.4 \pm 0.1 \text{ km s}^{-1}$ for Kepler-444A. We fit the relative RVs as a function of time and found a linear trend of $-7.8 \pm 0.5 \text{ m s}^{-1} \text{ yr}^{-1}$, where the uncertainty is derived adopting the rms of the fit (2.2 m s^{-1}) as the individual measurement error (Figure 2). This is consistent with, though somewhat smaller in amplitude, than the linear trend of $-11 \pm 5 \text{ km s}^{-1}$ reported by Sozzetti et al. (2009). In the following orbital analysis we use both our new, precise RV trend along with this value from the literature.

At three epochs, we also obtained HIRES spectra of the companion Kepler-444BC from which we obtained RVs by cross correlation with the well studied M dwarf Gl 699, resulting in two clear peaks. To extract the individual RVs of the two components of Kepler-444BC we simultaneously fit a two-component Gaussian to each peak in the cross-correlation functions. Table 3 reports our radial velocities for the components of Kepler-444BC. To derive the system velocity of the Kepler-444BC barycenter, we fit a linear relation to RV_B as a function of RV_C (Wilson 1941), and from the rms of the fit residuals we determine errors of 0.4 km s^{-1} in our deblended RVs for Kepler-444BC (Figure 3). We thus find a system velocity of $-123.05 \pm 0.17 \text{ km s}^{-1}$ and mass ratio of $M_C/M_B = 0.86 \pm 0.03$ for Kepler-444BC.

We estimated the potential amplitude of the Kepler-444BC photocenter orbit in our NIRC2 imaging given this mass ratio. In our K -band imaging we estimate the binary would have a flux ratio of $0.3 \pm 0.1 \text{ mag}$ based on the 0.4 mag ratio of cross-correlation function peaks in the optical RV data. The size of the photocenter orbit is defined as the total semimajor axis scaled down by the factor $f - \beta$, where $f \equiv M_C/(M_B + M_C) = 0.462 \pm 0.009$ and β is the ratio of secondary’s flux to the total flux ($\beta = 0.432 \pm 0.023$). We therefore expect the photocenter orbit to be 0.030 ± 0.024 times the size of the the semimajor axis. Since we detect no elongation at any epoch in our NIRC2 PSF-fitting, the semimajor axis is most likely to be $< 10 \text{ mas}$. We therefore expect the photocenter orbit to be $< 0.3 \text{ mas}$, which is smaller than the epoch-to-epoch uncertainty in the astrometric

calibration.

3. The Highly Eccentric Kepler-444A–BC Orbit

If the Kepler-444A–BC orbit has a semimajor axis close to its projected separation of 66 AU, its total orbital velocity would (on average) be 4.2 km s^{-1} , or 25 mas yr^{-1} , given its distance of 35.7 pc and a system mass of $1.30 M_{\odot}$. In contrast, we detect minimal astrometric motion ($-1.0 \pm 0.3 \text{ mas yr}^{-1}$ in separation, -0.002 ± 0.017 in PA) and a relatively small change in radial velocity ($\Delta \text{RV}_{\text{A–BC}} = -1.7 \pm 0.2 \text{ km s}^{-1}$). These measurements alone imply either that the A–BC orbit is eccentric and near apoastron or that it simply has a semimajor axis much larger than its projected separation. The detection of significant acceleration in Kepler-444A’s radial velocity favors the eccentric orbit scenario. To quantify the Kepler-444A–BC orbital parameters, we performed a Markov chain Monte Carlo (MCMC) joint analysis of our astrometric and RV data.

We used the Python implementation of the parallel-tempering ensemble sampler in `emcee v2.1.0` with 100 walkers and 30 temperatures. We found that parallel-tempering sampled our orbital parameter space more efficiently than the affine-invariant sampler (Foreman-Mackey et al. 2013) because a very wide range of orbits are consistent with our nearly stationary astrometry. We built up the initial starting points of our chains by iteratively adding in observational constraints. We began with a set of orbital parameters found by performing a separate Monte Carlo analysis of our astrometry, where we searched 10^6 randomly drawn values for orbital period (P), eccentricity (e), and time of periastron passage (T_0). As shown by Lucy (2014), combining astrometric measurements with this set of three parameters allows best-fit values for the other visual binary parameters to be determined in a least-squares sense. A subset of 10^3 of these trials having $\chi^2 - \chi_{\text{min}}^2 < 1$ were passed along to `emcee` as the starting points for our MCMC. After running `emcee` for 10^5 steps we added in the $\Delta \text{RV}_{\text{A–BC}}$ constraint, then after another 10^5 steps added in the RV linear trend measurements.

In our analysis, we fixed the distance at 35.7 pc but allowed for an uncertainty in the system mass of $1.30 \pm 0.06 M_{\odot}$. The asteroseismic analysis of Campante et al. (2015) determined the mass of Kepler-444A ($0.76 \pm 0.04 M_{\odot}$), and we use the mass–magnitude relation from Delfosse et al. (2000) to estimate masses of $0.29 \pm 0.03 M_{\odot}$ and $0.25 \pm 0.03 M_{\odot}$ for Kepler-444B and Kepler-444C based on their absolute magnitudes of $M_K = 6.91 \text{ mag}$ and 7.21 mag , respectively. The mass ratio of the A–BC system was fixed in our analysis to be $(M_B + M_C)/M_A = 0.71$. We adopted uniform priors in the logarithm of semimajor axis ($\log a$), eccentricity (e), argument of periastron (ω), PA of the ascending node (Ω), and mean longitude at the reference epoch of 2456511.83 JD (λ_{ref}). We assumed randomly distributed viewing angles by adopting an inclination prior uniform in $\cos i$. Finally, we imposed a “discovery prior” that was computed as the probability of detecting the binary companion in our $10'' \times 10''$ NIRC2 images at a random observation time. This effectively rules out extremely wide orbits ($>100''$) that only appear to have a small angular separation due to an improbable viewing angle. For a given semimajor axis (in angular units) this discovery prior

is only a function of e , i , and ω , so we interpolated the prior from a look-up table with grid steps of 0.03 in e , 3 deg in i , and 6 deg in ω . This prior has a relatively small impact on the results here, as it only affects orbital solutions with very large semimajor axes that match our astrometry well but do not match our RV data.

Figure 4 shows the six fitted parameters’ posterior distributions along with the most significant parameter correlations, and Table 4 gives the corresponding credible intervals for all orbital parameters of interest. We confirm that the A–BC orbit is indeed currently near apoastron, where it should spend most of its time, on a highly eccentric orbit ($e = 0.864 \pm 0.023$). The joint constraint from detecting almost no astrometric motion and our measurement of both velocity and acceleration orthogonal to the plane of the sky allows a remarkably precise determination of orbital parameters. For example, our MCMC gives an inclination of $i = 90.4_{-3.6}^{+3.4}$ deg. If we examine the best-fit orbits at assumed inclinations ranging from $i = 80$ deg to 100 deg, those orbits display PA motion of $0.057 \text{ deg yr}^{-1}$ to $-0.044 \text{ deg yr}^{-1}$. Our astrometry rules out such motion at 3.5σ and 2.5σ , respectively, even though the RVs computed from such orbits are quite consistent with our measurements.

4. Discussion

4.1. Dynamical Stability

We have found that the orbit of Kepler-444BC brings its center of mass within $5.0_{-1.0}^{+0.9}$ AU of Kepler-444A and its planetary system. Both the planetary and stellar orbits are subject to dynamical instabilities if the orbits are not sufficiently hierarchical. Extrapolation of empirical fits for stability of s-type planetary orbits from Holman & Wiegert (1999) suggest that the widest allowed planetary orbit around the primary is ≈ 1.6 AU, i.e., $20\times$ larger than the 0.08 AU orbit of Kepler-444f. This semi-major axis is likely an over estimate given that their fits do not consider hierarchical triples or orbits as eccentric as this. The existence of the triple stellar system itself also provides a stability constraint without considering the planets. According to Valtonen & Karttunen (2006), the triple system is stable as long as the tight pair Kepler-444BC has a semi-major axis less than 1.0 AU. This is consistent with the fact it was not resolved at any epoch of our Keck AO imaging (< 0.3 AU).

To assess the internal stability of the five-planet system, we estimated masses for the five planets from the Lissauer et al. (2011) mass–radius relation, $M/M_{\oplus} = (R/R_{\oplus})^{2.06}$. Campante et al. (2015) reported radii of $0.403_{-0.014}^{+0.016} R_{\oplus}$, $0.497_{-0.017}^{+0.021} R_{\oplus}$, $0.530_{-0.019}^{+0.022} R_{\oplus}$, $0.546_{-0.015}^{+0.017} R_{\oplus}$, and $0.74 \pm 0.04 R_{\oplus}$, in order from the innermost to outermost planet. We thereby compute planet masses of $0.15 M_{\oplus}$, $0.24 M_{\oplus}$, $0.27 M_{\oplus}$, $0.29 M_{\oplus}$, and $0.54 M_{\oplus}$, respectively. Even though the implied planet densities are high ($7\text{--}13 \text{ g cm}^{-3}$), we find that the planets masses are still low enough that they are spaced by 18–29 Hill radii, monotonically increasing outward. This is roughly twice the canonical limit at which mean motion resonance overlap drives multi-planet systems unstable (Chambers

et al. 1996). Therefore, we find that the planetary orbits should be quite stable in the absence of outside influences. Notably, planet pairs (a,b), (c,d), and (d,e) all fall near a 5:4 mean motion resonance, with (b,c) close to 4:3. Given the small masses, and the correspondingly small libration widths, this may not indicate present day resonant locking.

The high eccentricity of the A–BC stellar orbit pushes the bounds of the simulations on which published empirical stability fits are based, so we carried out direct n-body integrations tailored to match the properties of the Kepler-444 system. We used the publicly available Swifter integrator package (Levison & Duncan 2013) with the 15th order Gauss-Radau integrator (Everhart 1985). All of the planets were assigned their nominal semimajor axes, fixed star-planet mass ratios of 10^{-7} , and non-zero eccentricities and inclinations less than 10^{-3} and 1° respectively. We tested a range of eccentricities for the A–BC orbit, not just our measured value of $e = 0.864 \pm 0.023$, and for these other values of e we assumed that the binary is seen at 66 AU presently because it is at apocenter so that $a(1 + e) = 66$ AU. We also tested a range of mutual inclinations ranging from 0 – 70° . We found that even if the tighter B–C orbit is as wide as 0.3 AU, the planets were stable over Myr timescales for A–BC eccentricities as high as $e = 0.95$, i.e., corresponding to BC center-of-mass passages within 1.6 AU of the outermost planet. In this case, the planets’ eccentricities were excited to $\approx 10^{-2}$ by the interaction. Our n-body integrations cannot rule out much longer, Gyr-timescale instabilities due to secular resonance instabilities as this would require computationally expensive integrations and a broader parameter study beyond the scope of this work. More simplified secular models, which neglect the planetary masses, cannot capture the inclination evolution of the system (e.g., see Hamers & Portegies Zwart 2015). General relativistic effects and stellar tides, neglected here, may induce precession of the planets pericenter and tidal locking, but should not decrease orbital stability. We therefore conclude that our derived A–BC orbit is not ruled out by dynamical instabilities in the system.

4.2. Coplanarity of the Stellar and Planetary Orbits

A direct result from our analysis of the Kepler-444A–BC orbit is a measurement of the inclination, which we find to be consistent with edge-on ($i = 90.4_{-3.6}^{+3.4}$ deg). The inclinations measured by Campante et al. (2015) for the five planets are consistent with being internally coplanar within their errors, with the two most precise values being $87.96_{-0.31}^{+0.36}$ deg for Kepler-444f and 89.1 ± 0.5 deg for Kepler-444e.⁵ The planet orbits are then also consistent with having the same sky projected inclinations as the A–BC stellar orbit at $<1\sigma$. However, the planets could still have some mutual inclination with respect to the A–BC orbit. Directly constraining such mutual inclination requires

⁵Inclinations in the interval $i = 0$ – 90 deg correspond to counter-clockwise orbits, while the interval $i = 90$ – 180 deg corresponds to clockwise orbits. Transiting planets lack the information to distinguish between these two cases, unlike astrometric orbits, so transiting planet inclinations are reported in the interval $i = 0$ – 90 deg. In other words, the measurement for Kepler-444f could equivalently be interpreted as either $i = 89.1 \pm 0.5$ deg or $i = 90.9 \pm 0.5$ deg.

knowledge of the PA of the transiting planets’ orbits (i.e., their Ω), but this is observationally inaccessible. We therefore assess the likelihood of coplanarity from probabilistic arguments. The probability of having a sky projected inclination i by chance alone is $p(i) = \sin(i)/2$. Integrating this function we find a probability of randomly having an inclination within 4° of edge-on is 7%. This is the probability of the stellar orbit being observed with $i = 86\text{--}94^\circ$ if its mutual inclination with respect to the planetary orbits were in fact randomly oriented.

Our numerical integrations described in Section 4.1 offer a second probabilistic constraint on orbital alignments. When the A–BC orbit is not coplanar with the planetary orbits, precession is induced in the planets’ orbits. We find that the planets precess roughly as a rigid disk and cycle through states in which none or all of them appear to be transiting along a single sight line. We consider an initial configuration where the planet–BC inclination is entirely in the relative PA, with all planets transiting. This is a conservative initial condition in the sense that it will provide the most favorable configuration for transits. Because the planets precess like a rigid disk, the outermost planet is least likely to transit for a given inclination, and when the outer planet transits the interior planets do as well. The oscillation timescale of the planetary orbits is order a few $10^5\text{--}10^6$ yr, depending on the inclination. When the planet–BC orbit has an mutual inclination of 5° , all planets transit roughly 35% of the time. The fraction of time in transit drops to 25% for a mutual inclination of 10° . Although we do not carry out an exhaustive parameter study, some larger misalignments can provide slightly higher transit probabilities because the planetary orbits can become retrograde, as predicted by Li et al. (2014). Given our 2σ inclination uncertainty of 7° and that the five-planet system is transiting, we determine that the likelihood of misaligned stellar and planet orbits is $\approx 30\%$ from this second probabilistic constraint.

Combining these constraints, that we observe the planetary orbits to be edge on, the A–BC orbit to be edge on, and the five planets to be transiting today, we find a probability of only 2% that the Kepler-444 A–BC orbit is misaligned with respect to the planets. Therefore, we conclude that it is highly likely that the stellar A–BC and planetary orbits are coplanar within the range of our measurement uncertainties, providing an important constraint on the origin of the Kepler-444 system.

Finally, we note that the lack of eclipses between Kepler-444B and C in *Kepler* light curves does not rule out the Kepler-444B–C orbit being coplanar with the A–BC orbit and planet orbits within the observational uncertainties. The lack of eclipses only constrains their inclination to be $\Delta i = 0.5^\circ \left(\frac{R_B + R_C}{0.6 R_\odot}\right) \left(\frac{a}{0.3 \text{ AU}}\right)^{-1}$ away from edge-on ($89.5^\circ > i > 90.5^\circ$). Our numerical integrations indicate that moderate mutual inclinations between the B–C orbit and the planet orbits would induce only small amplitude precession ($\lesssim 1^\circ$) that would not cause the planets to ever go out of a transiting configuration.

4.3. Formation of the Triple Star System

We begin our discussion of plausible formation scenarios for the Kepler-444 system with the origin of the hierarchical triple stellar system. One of the most important questions is whether the triple system is primordial, by which we mean that it existed in its current orbital architecture at the epoch of planet formation. The three components may have initially formed in a less hierarchical, less eccentric configuration than observed today, through either core fragmentation or disk fragmentation. Observational evidence exists for both mechanisms (e.g., Pineda et al. 2015; Tobin et al., submitted). However, evolution into the system’s current state would have been rapid. A violent dynamical interaction could generate an eccentric triple due to an unstable orbital configuration at birth, typically occurring within 10^4 orbits ($\lesssim 10^6$ yr; Valtonen et al. 2008). In such cases, any interactions of the triple system with the initial gas cloud or protostellar disks would be concurrent with planet formation.

To arrive at the current hierarchical stellar arrangement at later times would most likely require the introduction of a fourth stellar body. Even in a relatively populous cluster (10^3 stars), simulations from Adams et al. (2006) indicate that encounters within 100 AU after 5 Myr are rare, occurring at a rate of $\approx 3 \times 10^{-4}$ star $^{-1}$ Myr $^{-1}$. If such an encounter occurred, the interaction needed to create the tight M dwarf pair would likely have required a violent, close passage destroying the planetary system. Moreover, the resulting alignment of the Kepler-444A–BC orbit would be expected to be random with respect to the planetary system around Kepler-444A, but we find they are coplanar (Section 4.2). Secular instabilities among the current three stars, such as the Kozai-Lidov mechanism, could cause orbital evolution over long timescales (Kozai 1962; Lidov 1962). However, dynamical stability requires that the M dwarf pair could not have been significantly wider in the past than it is today. Finally, even if there is or was an unknown fourth, wider companion, Kozai oscillations of the A–BC orbit are disfavored because the precession of the longitude of the pericenter driven by the A–BC system is faster than that driven by Kozai oscillations. We therefore conclude that it is highly improbable that the formation of the triple stellar system occurred at late times, so the A–BC orbit is very likely primordial.

4.4. Formation of the Planetary System

Given that the orbit of triple system was likely in place at or before the epoch of planet formation, we are then confronted with the fact that the protoplanetary disk would have been truncated by the M dwarf pair Kepler-444BC on their $a = 36.7_{-0.9}^{+0.7}$ AU, $e = 0.864 \pm 0.023$ orbit about the host star Kepler-444A. Extrapolating from the work of Artymowicz & Lubow (1994), we expect the disk to be truncated to 1–2 AU due to the close pericenter passage of 5 AU. Correctly modeling this truncation would require tailored modeling accounting for the specific triple system architecture here, so instead we conservatively adopt a truncation radius of 2 AU for the disk of Kepler-444A. The supply of solids available for planet formation would be severely limited in such

a disk. While continued feeding from an outer circum-triple ring is possible, as seen in systems such as GG Tau (Beck et al. 2012) or UY Aur (Stone et al. 2014), the eccentricity of the A–BC orbit makes this challenging. Not only would one expect a massive ring to damp the eccentricity of the orbit, but also the bulk of the material would accrete onto the BC components, rather than A (Young & Clarke 2015).

Adopting a minimum mass solar nebula (MMSN) gas surface density of $\Sigma = 1700 \text{ g/cm}^{-2} (\frac{r}{1 \text{ AU}})^{3/2}$ (Weidenschilling 1977; Hayashi 1981), and a 1:100 dust-to-gas mass ratio, the total mass of solids in Kepler-444A’s disk would have been $\approx 12 M_{\oplus}$. Given the fact that Kepler-444A is a metal-poor star ($[\text{Fe}/\text{H}] = -0.55$ dex), we might expect the dust-to-gas ratio to be $\approx 3\times$ smaller, implying a total mass budget of $\approx 4 M_{\oplus}$. Either case would require remarkably efficient conversion of dust to planets to create the five-planet system that has an estimated total mass of $1.5 M_{\oplus}$ (Section 4.1). In Figure 6 we compare the estimated planet masses to the predicted isolation mass of solids as a function of radius,

$$M_{\text{iso}} = \frac{(4\pi f_h \Sigma)^{3/2} r^3}{(3M_{\star})^{1/2}}, \quad (1)$$

where $f_h \approx 3.5$ is a geometric factor (Lissauer 1987). The isolation masses for a MMSN disk are far too low to support in situ formation, and also dust grains should have sublimated at the planets’ current locations. This is a familiar problem for Kepler systems, particularly for close-in super-Earths and Neptunes (e.g., Hansen & Murray 2012; Chiang & Laughlin 2013). For those more massive planets, local disk masses must be unphysically high (locally gravitationally unstable) to account for in-situ formation, implying either drifting in of solids or migration of fully formed planets (Schlichting 2014). Even with drifting of solids, disk mass measurements suggest that dust-to-planet conversion efficiencies may be quite high, depending on the amount of grain growth that previously occurred during the Class I phase (Najita & Kenyon 2014).

Current theories posit that close-in rocky planets, even super-Earths, may have formed near their current orbital locations by delivery of solids from much larger disk radii (Chatterjee & Tan 2014; Lee et al. 2014). A pressure maximum located at the boundary between the MRI-active zone and the disk deadzone could provide a plausible trap for the collection of solids. This deadzone boundary is thought to occur at $\approx 0.1 \text{ AU}$ and is expected to have weak to no dependence on metallicity (Martin et al. 2012; Mohanty et al. 2013). At the pressure maximum, pebbles drifting in from large radii collect and can either coalesce through a ring instability in the solids, streaming instabilities, or coagulation. Sequential epochs of pebble gathering could thus produce multiple low mass planets in this so-called “inside-out” planet formation model.

The five Kepler-444 planets, among the smallest discovered by *Kepler*, appear to be qualitatively consistent with in-situ, drift-aided planet formation occurring in a truncated disk. The mass reservoir was severely depleted, which would have resulted in less material being delivered to the deadzone edge. The material would also likely have been depleted in volatiles, since the disk would have been truncated within or very near to the ice-line. Therefore, the planets formed here might have been expected to be smaller, and denser than those formed via “inside-out” planet

formation in a normal disk around a single star. The monotonic size ordering is consistent with this scenario and should not be due to distance dependent mass loss via oblation (Perez-Becker & Chiang 2013), as even the innermost planet has too low an equilibrium temperature (<1500 K) for this to be applicable. The innermost planet orbits roughly a factor of two closer than the expected formation site at the deadzone boundary. Type I migration might have caused inward drift from that formation site toward the disk’s inner edge, as the estimated planet masses ($0.15\text{--}0.54 M_{\oplus}$) are well below the gap-opening mass.

Despite these qualitative successes, there is still a quantitative mass budget problem for a truncated MMSN disk. However, unlike most other Kepler systems, the Kepler-444 planets are small enough that a disk with only $20\times$ the surface density of the MMSN at 1 AU would have sufficiently high isolation masses to form the planets locally (albeit at $\sim 100\%$ efficiency) without relying on any material from the outer disk. More conservatively, this more massive disk would contain $80\text{--}240 M_{\oplus}$ of solid material within 2 AU, depending on the dust-to-gas ratio. This total supply of solid material would then require only $\lesssim 2\%$ efficiency in planet formation, assuming it could be delivered to the inner disk as described above.

If the solution to the overall mass budget problem is an unusually massive disk, this might hint at a coherent formation model for both the hierarchical triple and the planets. While a disk 20 times as massive as the MMSN would be locally stable to gravitational instabilities, when extrapolated out to typical disk radii of ~ 100 AU (Andrews et al. 2013), the total disk mass would approach that of the primary star. At large radii ($70\text{--}100$ AU) temperatures are low ($40\text{--}50$ K), and thus a massive disk would likely become gravitationally unstable and susceptible to fragmentation (Adams et al. 1989; Kratter et al. 2010b). Numerical simulations show that disks with such high disk-to-star mass ratios usually fragment into 1–2 objects that grow to high mass ratios relative to the host star by successfully competing for accreting material from the disk and envelope (Stamatellos & Whitworth 2009; Krumholz et al. 2007; Kratter et al. 2010a). The rapid growth of fragments formed in the outer disk naturally leads to rapid dynamical evolution with varied outcomes, including ejection, merging, and inward or outward migration. One possible outcome of these interactions is an eccentric close binary pair orbiting the primary, resembling the Kepler-444ABC system (Stamatellos & Whitworth 2009; Zhu et al. 2012). A disk origin for the triple star system and close-in planets is also consistent with the fact that the planetary and A–BC orbits seem to be coplanar, although other primordial formation modes could potentially bring the protoplanetary disk into alignment with the triple within the lifetime of the disk (Bate et al. 2000).

The key challenge to this disk fragmentation scenario is that observations indicate that such massive disks are not typical (e.g., Mann et al. 2015), although massive disks with star-to-disk mass ratios close to unity seem to exist (Tobin et al. 2012). Such a scenario is at least plausible for the Kepler-444 system, which has a total stellar mass of $1.3 M_{\odot}$, as Kratter et al. (2008) showed that protostellar cores with sufficient mass to produce bound system masses of about $1.5 M_{\odot}$ are marginally unstable to disk fragmentation.

5. Conclusions

We present the first results from our Keck/NIRC2 AO astrometry program investigating the orbital architectures of planet hosting multiple systems. Kepler-444 is a hierarchical triple star system with five sub-Earth sized planets in orbit about the primary star. Combining our Keck/NIRC2 astrometry with Keck/HIRES RVs of all three stellar components, we determine that the orbit of the center of mass of Kepler-444BC about Kepler-444A is highly eccentric ($e = 0.864 \pm 0.023$) with a pericenter passage of only $5.0_{-1.0}^{+0.9}$ AU. We also find that this stellar orbit is consistent with being edge-on within the measurement uncertainties ($i = 90.4_{-3.6}^{+3.4}$ deg), making it very likely to be coplanar with the planetary system given the low probability of a misaligned orbit appearing to be this close to edge-on. Through direct n-body integrations we validate that this orbital configuration is dynamically stable both for the triple star system and five planet system.

We consider a variety of formation scenarios that can simultaneously explain both the origin of the stellar system (total mass $1.3 M_{\odot}$) and the existence of the tiny planets on small orbits (total mass $\approx 1.5 R_{\oplus}$). We conclude that:

- The stellar orbit is most likely to be primordial, i.e., in place at or before the epoch of planet formation in the system.
- The protoplanetary disk from which the planets formed would have been truncated at 1–2 AU, severely depleting the reservoir of solid material available to form the observed planets. This truncation would have occurred near the ice line, removing most if not all volatiles from the descendant planets.
- The small masses are consistent with some in-situ planet formation models, for example the “inside out” model. This system reinforces the idea that more typical Kepler systems, possessing larger planets than seen here, are built by accumulation of solids drifting in from large disk radii. For the truncated disk of Kepler-444, a MMSN scaled up by $20\times$ would have adequate solid mass within 2 AU even at low metallicity ($80 M_{\oplus}$) to produce these planets at 2% efficiency.
- If the natal disk was indeed this massive, the outer regions of the disk would have originally been unstable to gravitational fragmentation. Therefore, if such a massive disk is needed to solve the mass budget problem, then the triple system might have naturally arisen from disk fragments that rapidly evolved dynamically into a highly eccentric, coplanar orbital configuration, consistent with our observations.

The Kepler-444 system would appear to be a hostile environment in which to form planets. The host star is metal poor, $[\text{Fe}/\text{H}] = -0.55$ dex, and we have shown that the stellar companions Kepler-444BC would have severely inhibited planet formation in the protoplanetary disk. Yet five planets, albeit small ones, did form here. This may imply that the assembly of sub-Earth-sized planets is quite robust, particularly in single star systems with meager disks possessing a reduced

supply of solids. However, if our suggested formation pathway requiring an unusually massive disk is correct, then the planet outcome seen here may not be typical of most multiple star systems that have companions on solar system scales ($\sim 10\text{--}100$ AU). Future work to build a large sample of stellar orbit determinations in planet-hosting binary systems will be key to better understand these fundamental issues for planet formation.

This work was supported by a NASA Keck PI Data Award, administered by the NASA Exoplanet Science Institute. KMK was supported by NSF AST-1410174. We thank Will Best for assistance with some Keck/NIRC2 observations. It is a pleasure to thank Joel Aycocock, Carolyn Jordan, Jason McIlroy, Luca Rizzi, Terry Stickel, Hien Tran, and the Keck Observatory staff for assistance with our Keck AO observations. The HIRES data presented here were obtained in collaboration with Geoff Marcy. We also thank James R. A. Davenport for distributing his IDL implementation of the cubehelix color scheme (Green 2011). Our research has employed the 2MASS data products; NASA’s Astrophysical Data System; and the SIMBAD database operated at CDS, Strasbourg, France. Finally, the authors wish to recognize and acknowledge the very significant cultural role and reverence that the summit of Mauna Kea has always had within the indigenous Hawaiian community. We are most fortunate to have the opportunity to conduct observations from this mountain.

Facilities: Keck:II (NGS AO, NIRC2)

REFERENCES

- Adams, E. R., Ciardi, D. R., Dupree, A. K., Gautier, III, T. N., Kulesa, C., & McCarthy, D. 2012, *AJ*, 144, 42
- Adams, E. R., Dupree, A. K., Kulesa, C., & McCarthy, D. 2013, *AJ*, 146, 9
- Adams, F. C., Proszkow, E. M., Fatuzzo, M., & Myers, P. C. 2006, *ApJ*, 641, 504
- Adams, F. C., Ruden, S. P., & Shu, F. H. 1989, *ApJ*, 347, 959
- Andrews, S. M., Rosenfeld, K. A., Kraus, A. L., & Wilner, D. J. 2013, *ApJ*, 771, 129
- Artymowicz, P., & Lubow, S. H. 1994, *ApJ*, 421, 651
- Bate, M. R., Bonnell, I. A., Clarke, C. J., Lubow, S. H., Ogilvie, G. I., Pringle, J. E., & Tout, C. A. 2000, *MNRAS*, 317, 773
- Bechter, E. B., et al. 2014, *ApJ*, 788, 2
- Beck, T. L., Bary, J. S., Dutrey, A., Piétu, V., Guilloteau, S., Lubow, S. H., & Simon, M. 2012, *ApJ*, 754, 72
- Borucki, W. J., et al. 2010, *Science*, 327, 977
- Butler, R. P., et al. 2006, *ApJ*, 646, 505
- Campante, T. L., et al. 2015, *ApJ*, 799, 170
- Chambers, J. E., Wetherill, G. W., & Boss, A. P. 1996, *Icarus*, 119, 261
- Chatterjee, S., & Tan, J. C. 2014, *ApJ*, 780, 53
- Chiang, E., & Laughlin, G. 2013, *MNRAS*, 431, 3444
- Cieza, L. A., et al. 2009, *ApJ*, 696, L84
- Delfosse, X., Forveille, T., Ségransan, D., Beuzit, J.-L., Udry, S., Perrier, C., & Mayor, M. 2000, *A&A*, 364, 217
- Diolaiti, E., Bendinelli, O., Bonaccini, D., Close, L., Currie, D., & Parmeggiani, G. 2000, *A&AS*, 147, 335
- Doyle, L. R., et al. 2011, *Science*, 333, 1602
- Dupuy, T. J., Liu, M. C., Bowler, B. P., Cushing, M. C., Helling, C., Witte, S., & Hauschildt, P. 2010, *ApJ*, 721, 1725
- Dupuy, T. J., Liu, M. C., & Ireland, M. J. 2009, *ApJ*, 692, 729

- . 2014, *ApJ*, 790, 133
- Eastman, J. D., et al. 2015, ArXiv e-prints
- Everett, M. E., Barclay, T., Ciardi, D. R., Horch, E. P., Howell, S. B., Crepp, J. R., & Silva, D. R. 2015, *AJ*, 149, 55
- Everhart, E. 1985, in *Dynamics of Comets: Their Origin and Evolution*, Proceedings of IAU Colloq. 83, held in Rome, Italy, June 11-15, 1984. Edited by Andrea Carusi and Giovanni B. Valsecchi. Dordrecht: Reidel, *Astrophysics and Space Science Library*. Volume 115, 1985, p.185, ed. A. Carusi & G. B. Valsecchi, 185
- Foreman-Mackey, D., Hogg, D. W., Lang, D., & Goodman, J. 2013, *PASP*, 125, 306
- Ghez, A. M., White, R. J., & Simon, M. 1997, *ApJ*, 490, 353
- Green, D. A. 2011, *Bulletin of the Astronomical Society of India*, 39, 289
- Hamers, A. S., & Portegies Zwart, S. F. 2015, ArXiv e-prints
- Hansen, B. M. S., & Murray, N. 2012, *ApJ*, 751, 158
- Harris, R. J., Andrews, S. M., Wilner, D. J., & Kraus, A. L. 2012, *ApJ*, 751, 115
- Hatzes, A. P., Cochran, W. D., Endl, M., McArthur, B., Paulson, D. B., Walker, G. A. H., Campbell, B., & Yang, S. 2003, *ApJ*, 599, 1383
- Hayashi, C. 1981, *Progress of Theoretical Physics Supplement*, 70, 35
- Heppenheimer, T. A. 1974, *Icarus*, 22, 436
- Holman, M. J., & Wiegert, P. A. 1999, *AJ*, 117, 621
- Howard, A. W., et al. 2010, *ApJ*, 721, 1467
- Jang-Condell, H., Mugrauer, M., & Schmidt, T. 2008, *ApJ*, 683, L191
- Kozai, Y. 1962, *AJ*, 67, 591
- Kratter, K. M., Matzner, C. D., & Krumholz, M. R. 2008, *ApJ*, 681, 375
- Kratter, K. M., Matzner, C. D., Krumholz, M. R., & Klein, R. I. 2010a, *ApJ*, 708, 1585
- Kratter, K. M., Murray-Clay, R. A., & Youdin, A. N. 2010b, *ApJ*, 710, 1375
- Kraus, A. L., Ireland, M. J., Hillenbrand, L. A., & Martinache, F. 2012, *ApJ*, 745, 19
- Kraus, A. L., Ireland, M. J., Martinache, F., & Hillenbrand, L. A. 2011, *ApJ*, 731, 8
- Krumholz, M. R., Klein, R. I., & McKee, C. F. 2007, *ApJ*, 656, 959

- Lee, E. J., Chiang, E., & Ormel, C. W. 2014, *ApJ*, 797, 95
- Levison, H. F., & Duncan, M. J. 2013, SWIFT: A solar system integration software package, *Astrophysics Source Code Library*
- Li, G., Naoz, S., Kocsis, B., & Loeb, A. 2014, *ApJ*, 785, 116
- Lidov, M. L. 1962, *Planet. Space Sci.*, 9, 719
- Lillo-Box, J., Barrado, D., & Bouy, H. 2014, *A&A*, 566, A103
- Lissauer, J. J. 1987, *Icarus*, 69, 249
- Lissauer, J. J., et al. 2011, *ApJS*, 197, 8
- Lucy, L. B. 2014, *A&A*, 563, A126
- Mann, R. K., Andrews, S. M., Eisner, J. A., Williams, J. P., Meyer, M. R., Di Francesco, J., Carpenter, J. M., & Johnstone, D. 2015, *ApJ*, 802, 77
- Martin, R. G., Lubow, S. H., Livio, M., & Pringle, J. E. 2012, *MNRAS*, 420, 3139
- Mohanty, S., Ercolano, B., & Turner, N. J. 2013, *ApJ*, 764, 65
- Najita, J. R., & Kenyon, S. J. 2014, *MNRAS*, 445, 3315
- Perez-Becker, D., & Chiang, E. 2013, *MNRAS*, 433, 2294
- Pineda, J. E., et al. 2015, *Nature*, 518, 213
- Rafikov, R. R. 2015, *ApJ*, 804, 62
- Schlichting, H. E. 2014, *ApJ*, 795, L15
- Silsbee, K., & Rafikov, R. R. 2015, *ApJ*, 798, 71
- Sozzetti, A., Torres, G., Latham, D. W., Stefanik, R. P., Korzennik, S. G., Boss, A. P., Carney, B. W., & Laird, J. B. 2009, *ApJ*, 697, 544
- Stamatellos, D., & Whitworth, A. P. 2009, *MNRAS*, 392, 413
- Stone, J. M., Eisner, J. A., Salyk, C., Kulesa, C., & McCarthy, D. 2014, *ApJ*, 792, 56
- Tobin, J. J., Hartmann, L., Chiang, H.-F., Wilner, D. J., Looney, L. W., Loinard, L., Calvet, N., & D'Alessio, P. 2012, *Nature*, 492, 83
- Valtonen, M., & Karttunen, H. 2006, *The Three-Body Problem*
- Valtonen, M., Mylläri, A., Orlov, V., & Rubinov, A. 2008, in *IAU Symposium*, Vol. 246, IAU Symposium, ed. E. Vesperini, M. Giersz, & A. Sills, 209–217

- van Leeuwen, F. 2007, *Hipparcos, the New Reduction of the Raw Data (Hipparcos, the New Reduction of the Raw Data. By Floor van Leeuwen, Institute of Astronomy, Cambridge University, Cambridge, UK Series: Astrophysics and Space Science Library, Vol. 350 20 Springer Dordrecht)*
- Wang, J., Fischer, D. A., Xie, J.-W., & Ciardi, D. R. 2014, *ApJ*, 791, 111
- . 2015, *ArXiv e-prints*
- Weidenschilling, S. J. 1977, *Ap&SS*, 51, 153
- Welsh, W. F., et al. 2012, *Nature*, 481, 475
- White, R. J., & Ghez, A. M. 2001, *ApJ*, 556, 265
- Wilson, O. C. 1941, *ApJ*, 93, 29
- Wizinowich, P., et al. 2000, *PASP*, 112, 315
- Yelda, S., Lu, J. R., Ghez, A. M., Clarkson, W., Anderson, J., Do, T., & Matthews, K. 2010, *ApJ*, 725, 331
- Youdin, A. N., & Goodman, J. 2005, *ApJ*, 620, 459
- Young, M. D., & Clarke, C. J. 2015, *MNRAS*, 452, 3085
- Zhu, Z., Hartmann, L., Nelson, R. P., & Gammie, C. F. 2012, *ApJ*, 746, 110

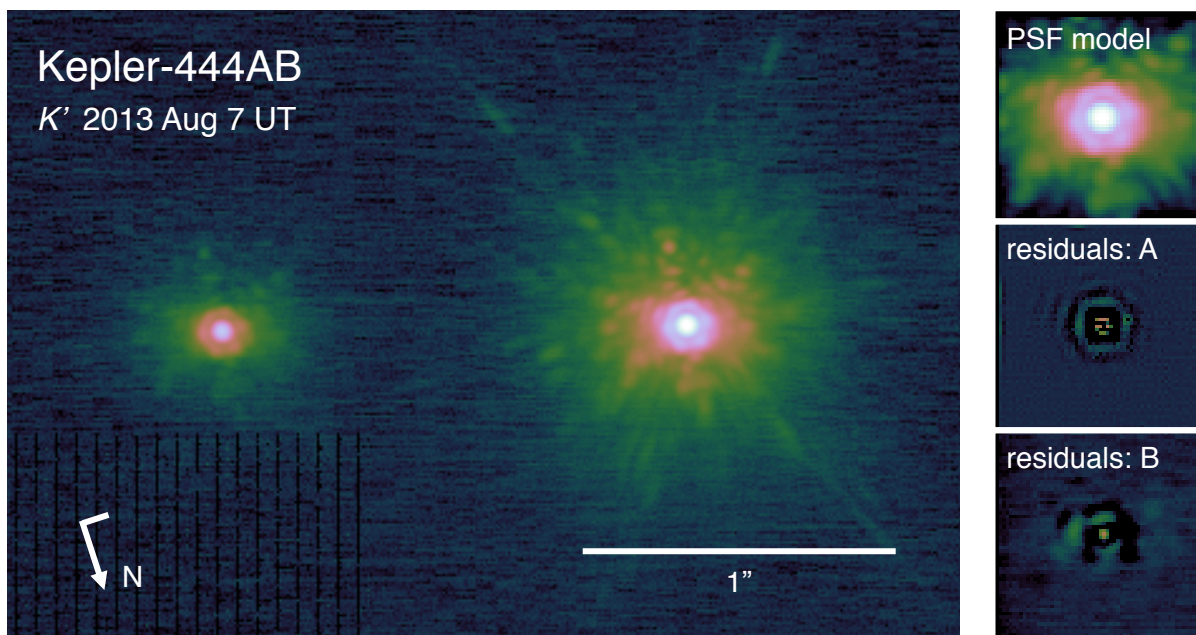


Fig. 1.— Left: an example of one of our Keck/NIRC2 NGS AO images of Kepler-444AB. Right: results of our StarFinder PSF-modeling of this image showing the best-fit PSF model (top), and residuals when subtracting this from the primary (middle) and secondary (bottom) components. Kepler-444B is known to be a double-lined spectroscopic binary, but we do not resolve it (<10 mas) at any of our four observation epochs.

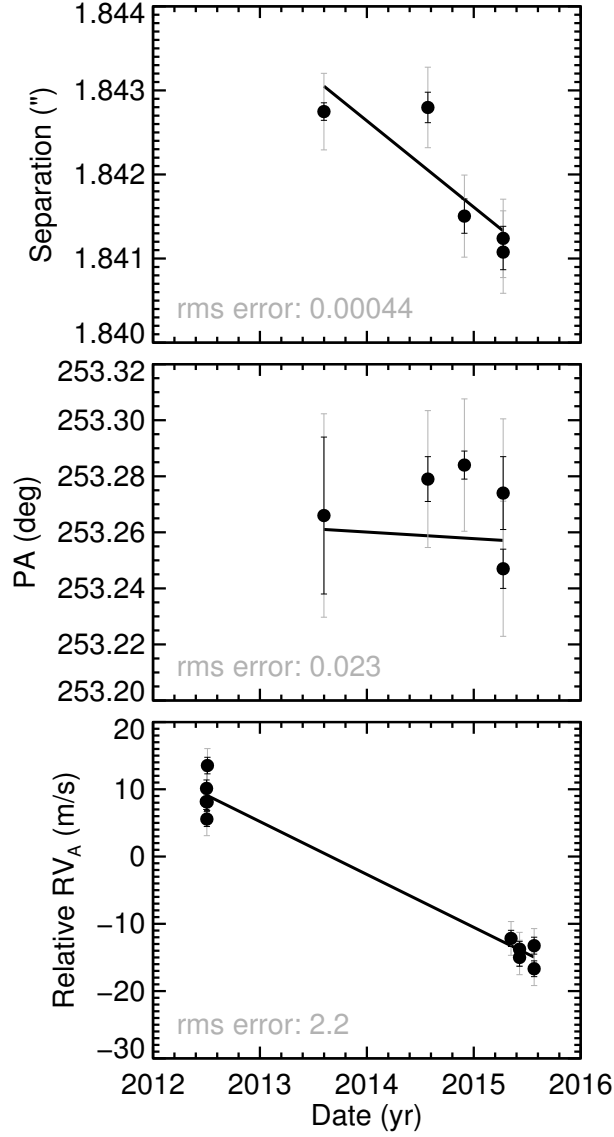


Fig. 2.— Astrometric and RV monitoring data shown alongside linear fits to the data as a function of time (see Table 4 for the coefficients). In each plot the smaller black error bars are the nominal errors (computed from the rms of individual dithers for astrometry). The larger gray error bars are the total errors computed from the rms about the fit, which should include for example errors in astrometric calibration of NIRC2. The value of this rms error is given in the bottom left of each panel. The astrometry is nearly stationary, indicating very little motion in the plane of the sky ($\lesssim 1 \text{ mas yr}^{-1}$; $\lesssim 0.2 \text{ km s}^{-1}$), while RV monitoring of the planet hosting primary star reveals an acceleration in the orthogonal direction due to A–BC orbital motion.

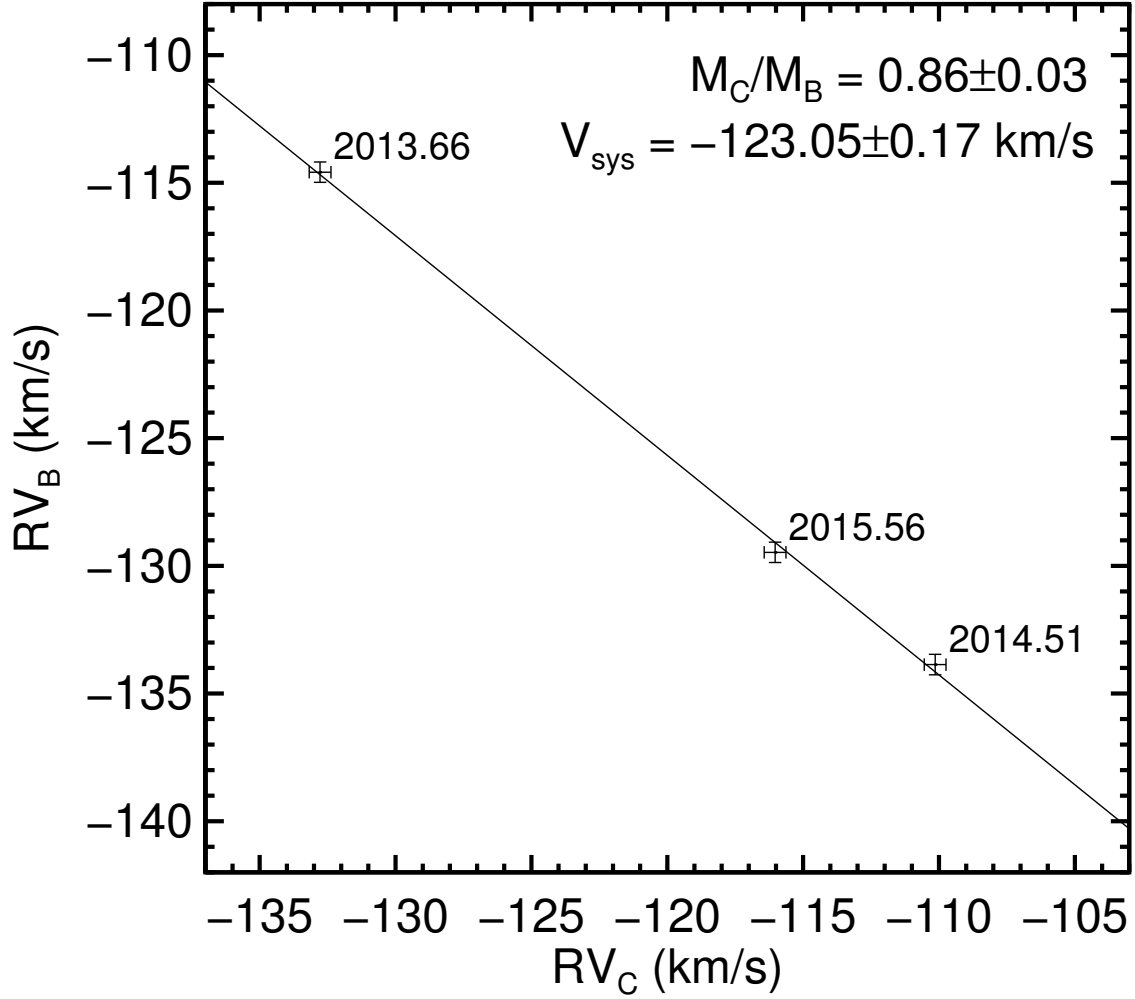


Fig. 3.— Radial velocities for the spectroscopic binary companion system Kepler-444BC. Even without a full orbit fit, a linear fit to RV_C as a function of RV_B is sufficient to determine the system velocity and mass ratio (Wilson 1941). By combining this system velocity ($RV_{BC} = -123.05 \pm 0.17 \text{ km s}^{-1}$) with the known RV of the primary ($RV_A = -121.4 \pm 0.1 \text{ km s}^{-1}$) we derive a ΔRV of $-1.7 \pm 0.2 \text{ km s}^{-1}$. We therefore detect significant orbital motion orthogonal to the plane of the sky, even though our astrometry shows almost no motion ($\lesssim 1 \text{ mas yr}^{-1}$; $\lesssim 0.2 \text{ km s}^{-1}$).

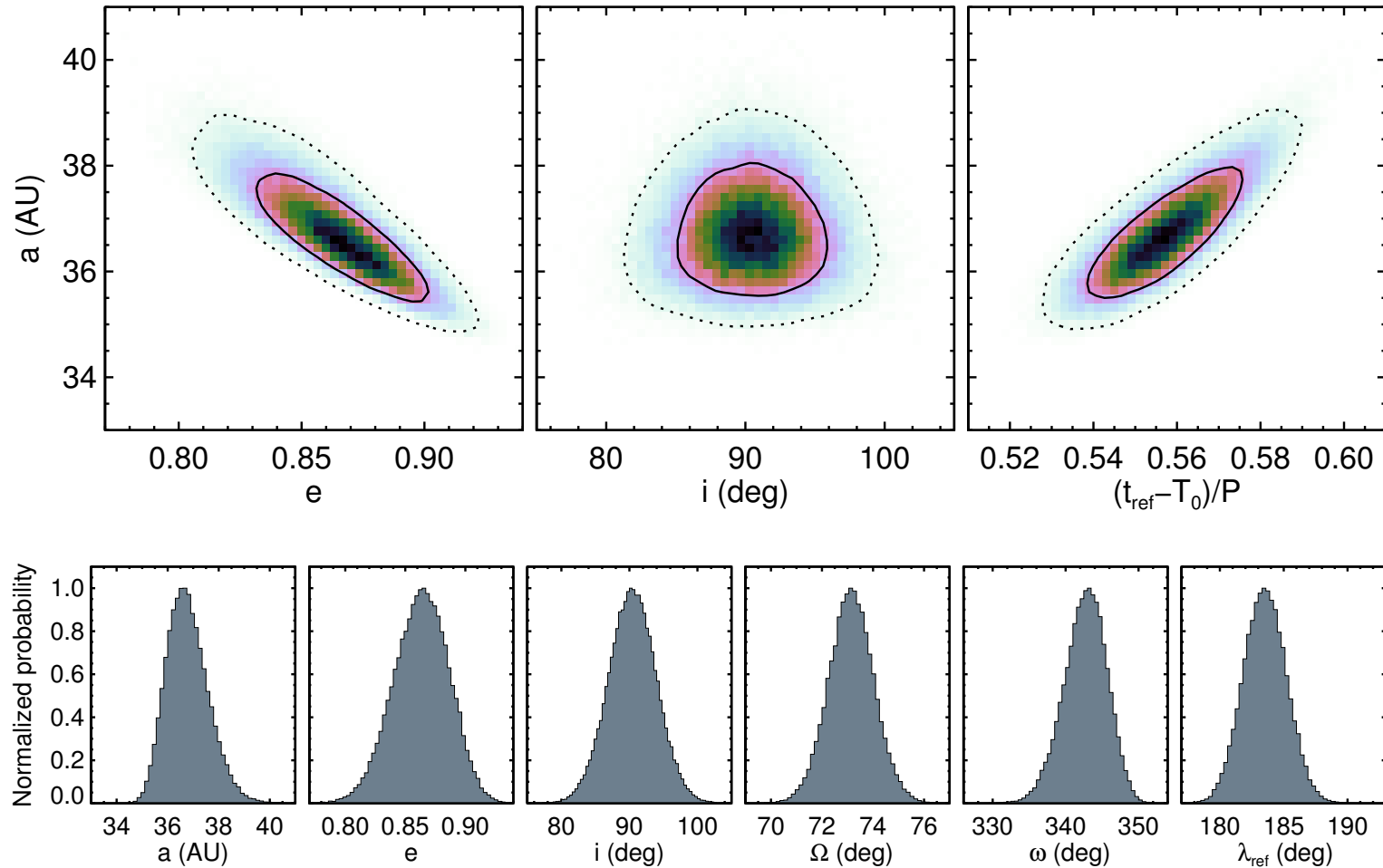


Fig. 4.— MCMC posterior distributions for the properties of the orbit of Kepler-444BC around Kepler-444A. Top: parameter correlations shown as 2-d probability density, with contours indicating 1σ (solid) and 2σ (dotted) regions. Bottom: marginalized posteriors of all 6 fitted orbital parameters. Kepler-444AB is currently at a projected separation of 66 AU because it is in fact a highly eccentric, 37 AU binary that is near apoastron and that is also consistent with being seen edge on (defined as $i = 90$ deg). Apoastron is defined as $(t - T_0)/P = 0.5$, and we have defined t_{ref} as the first epoch of Keck astrometry on 2013 Aug 7 UT. Bottom: marginalized posterior distributions for each of the six fitted orbital parameters.

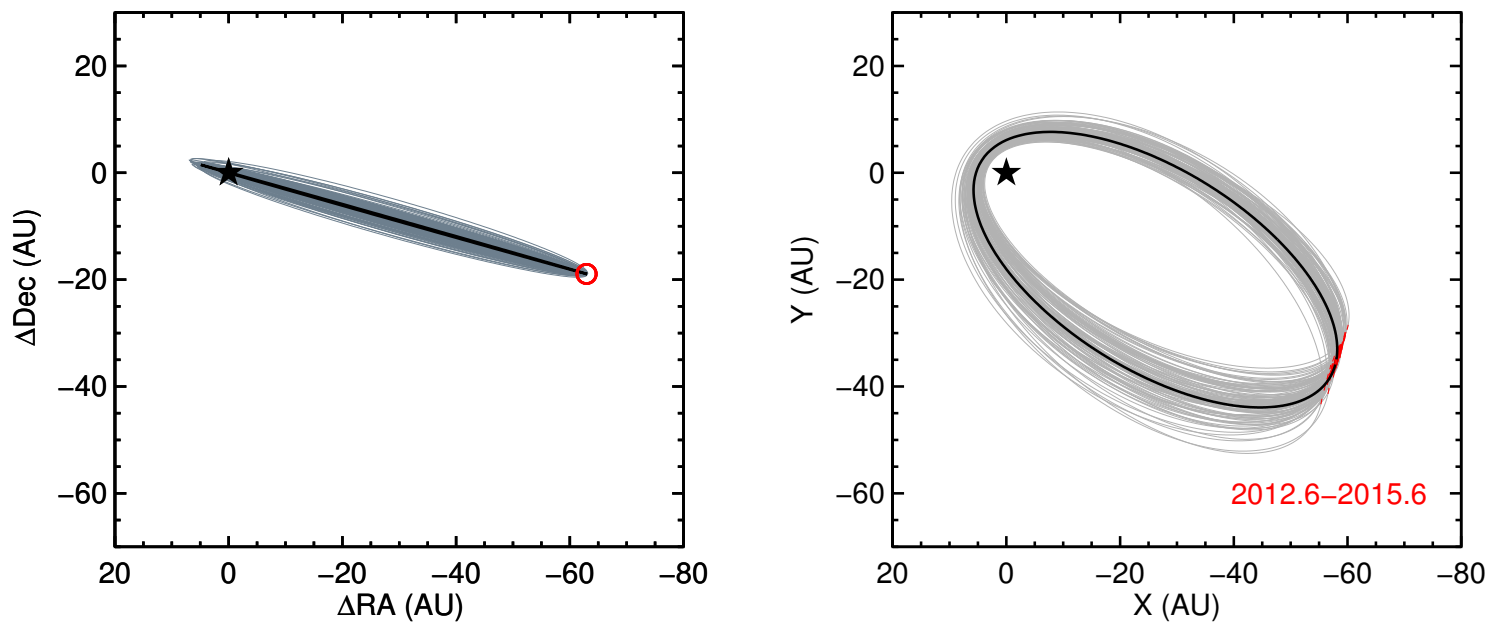


Fig. 5.— The orbit of the Kepler-444BC system in the frame of the planet host star Kepler-444A (black star). Our best-fit orbit is shown in black, and 100 randomly drawn orbits from our MCMC analysis are shown in gray. Orbit locations that correspond to the range of our observation epochs are shown in red. Left: the orbit in plane of the sky, which is consistent with being seen edge on. Right: the same orbits shown deprojected in a top down view of the orbital plane. The orbit is currently close to apoastron with almost no motion in the plane of the sky.

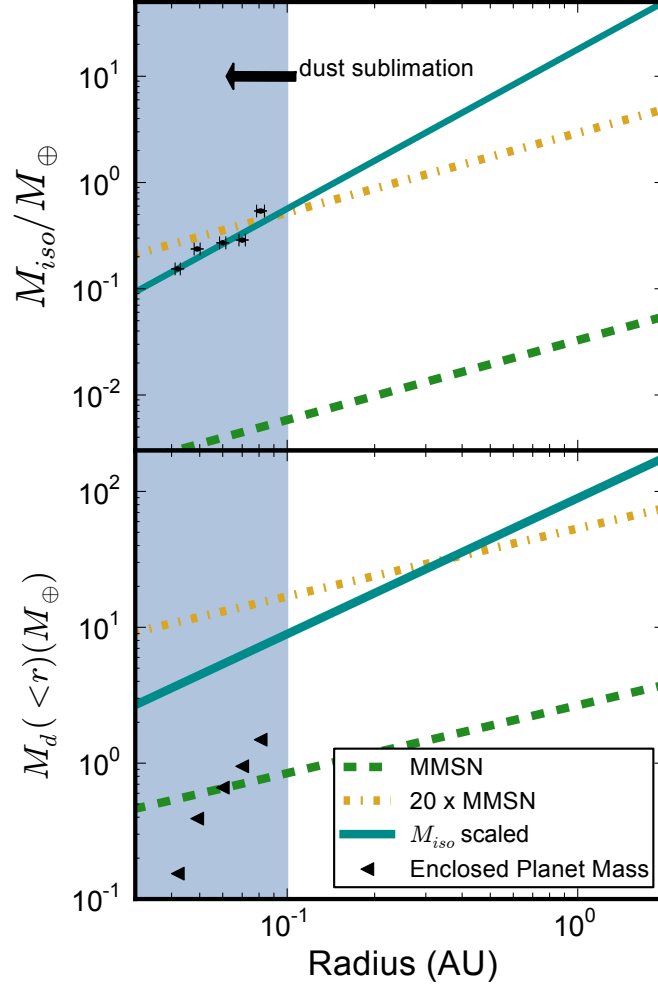


Fig. 6.— Top: comparison of the estimated planet masses to the isolation mass of solids (M_{iso}) as a function of disk radius for three protoplanetary disk models. The green dashed line is a MMSN disk with $\Sigma_{\text{gas}} = 1700\text{g/cm}^{-2}$ at 1 AU, a surface density profile $\Sigma \propto r^{-3/2}$, and a dust-to-gas ratio of 1:300. The gold dash-dotted line is the same MMSN scaled up by a factor of 20. The solid blue line shows that a shallower surface density profile, $\Sigma \propto r^{-1}$, produces isolation masses that increase more similarly to the planet masses. The x -axis error bars on planet masses indicate the size of the feeding zone of each planet, demonstrating that though packed, they do not overlap. Bottom: the total enclosed mass in these three disk models as a function of disk radius. Black triangles show the total enclosed planet mass. Both the M_{iso} -scaled disk and the $20\times$ MMSN models are consistent with disk masses that would lead to gravitational instability at 50–100 AU.

Table 1. Keck/NIRC2 NGS AO Astrometry for Kepler-444AB

Date (UT)	Filter	Separation (mas)	PA (deg)
2013 Aug 7	K'	1842.75 ± 0.10	253.266 ± 0.028
2014 Jul 28	K_{cont}	1842.80 ± 0.18	253.279 ± 0.008
2014 Nov 30	K_{cont}	1841.51 ± 0.20	253.284 ± 0.005
2015 Apr 11	K_{cont}	1841.24 ± 0.14	253.247 ± 0.007
2015 Apr 11	K_{cont}	1841.08 ± 0.21	253.274 ± 0.013

Note. — Uncertainties quoted here are simply the rms of measurements obtained from individual images at each epoch and do not account for potential systematic errors (e.g., due to uncertainties in the distortion correction, pixel scale and orientation). There are two distinct measurements at the 2015 Apr 11 epoch because data were obtained at different NIRC2 orientations placing the binary components on different pixel positions on the detector and thus experiencing different distortion offsets.

Table 2. Keck/HIRES Relative Radial Velocities for Kepler-444A

Date (JD)	RV_A (m s^{-1})
2456109.920	8.17 ± 1.2
2456110.831	10.13 ± 1.3
2456111.897	5.57 ± 1.1
2456112.869	8.11 ± 1.3
2456113.809	13.53 ± 1.2
2457151.099	-12.17 ± 1.2
2457180.106	-15.00 ± 1.3
2457180.109	-13.76 ± 1.2
2457229.929	-13.25 ± 1.3
2457229.932	-16.68 ± 1.2

Table 3. Keck/HIRES Radial Velocities for Kepler-444BC

Date (JD)	RV_B (km s^{-1})	RV_C (km s^{-1})
2456532.7	-114.6 ± 0.4	-132.8 ± 0.4
2456845.0	-133.9 ± 0.4	-110.1 ± 0.4
2457229.9	-129.5 ± 0.4	-116.0 ± 0.4

Note. — Uncertainties quoted here were determined from the rms of our fit of RV_B as a function of RV_C .

Table 4. MCMC Results for the Orbit of Kepler-444AB

Property	Median $\pm 1\sigma$	Notes/Prior
Input measurements		
Separation, ρ (mas)	1843.0 ± 0.4	A
$\dot{\rho}$ (mas yr $^{-1}$)	-1.0 ± 0.3	A
PA, θ (deg)	253.258 ± 0.021	A
$\dot{\theta}$ (deg yr $^{-1}$)	-0.002 ± 0.017	A
ΔRV_{BC-A} (km s $^{-1}$)	-1.7 ± 0.2	B
$R\dot{V}_A$ (m s $^{-1}$ yr $^{-1}$)	-7.8 ± 0.5	C
$R\dot{V}_A$ (m s $^{-1}$ yr $^{-1}$)	-11 ± 5	D
System mass, M_{tot} (M_{\odot})	1.30 ± 0.06	E
A–BC mass ratio, $(M_B + M_C)/M_A$	0.71 (fixed)	E
Distance, d (pc)	35.7 (fixed)	<i>Hipparcos</i>
Output posteriors		
Semimajor axis, a (AU)	$36.7^{+0.7}_{-0.9}$	$1/a$ (log-flat)
Eccentricity, e	0.864 ± 0.023	uniform
Inclination, i (deg)	$90.4^{+3.4}_{-3.6}$	$\sin(i)$
PA of the ascending node, Ω (deg)	73.1 ± 0.9	uniform
Argument of periastron, ω (deg)	$342.8^{+3.2}_{-2.6}$	uniform
Mean longitude at 2456511.83 JD, λ_{ref} (deg)	183.5 ± 1.7	uniform
Period, $P = \sqrt{a^3/M_{\text{tot}}}$ (yr)	198^{+8}_{-9}	...
Time of periastron, $T_0 = t_{\text{ref}} - (\lambda_{\text{ref}} - \omega)P/2\pi$ (JD)	2488500 ± 900	...
Closest approach during periastron, $a(1 - e)$ (AU)	$5.0^{+0.9}_{-1.0}$...

Note. — The reference epoch for λ_{ref} is $t_{\text{ref}} = 2456511.83$ JD (2013 Aug 7 UT). Notes on input measurements: (A) astrometry corresponds to the epoch range 2456511.83 JD to 2457124.13 JD; (B) ΔRV_{BC-A} corresponds to epoch 2456532.74 JD; (C) our HIRES linear RV trend corresponds to the epoch range 2456109.92 JD to 2457229.93 JD; (D) RV trend from Sozzetti et al. (2009) corresponds to the epoch range 2452812.02 JD to 2453568.85 JD; (E) Campante et al. (2015) give a mass for Kepler-444A of $0.76 \pm 0.04 M_{\odot}$ from their asteroseismic analysis, and we estimate masses for Kepler-444B and C of $0.29 \pm 0.03 M_{\odot}$ and $0.25 \pm 0.03 M_{\odot}$, respectively, from the Delfosse et al. (2000) mass–magnitude relation.